



Comparison of Buckling Distortion Propensity for SAW, GMAW, and FSW

Analysis revealed a correlation between residual stress distribution and the type of welding distortion

BY S. R. BHIDE, P. MICHALERIS, M. POSADA, AND J. DELOACH

ABSTRACT. Welding induces residual stresses in welded structures that result in bowing, angular, and buckling distortions. The magnitude of longitudinal residual stress is critical in predicting the onset of buckling distortion, which affects numerous welding applications in the shipbuilding, railroad, and other industries. This paper compares submerged arc welding (SAW), gas metal arc welding (GMAW), and friction stir welding (FSW) in terms of their buckling propensity by measuring the longitudinal residual stresses on HSLA-65 steel welded plates of identical dimensions. The blind hole drilling method was used to measure the longitudinal residual stress and distortion measurements were obtained by using digital gauges at 40 points on the plates. Analyses of the longitudinal residual stresses and distortion measurements revealed that the FS-welded plate has buckling distortion, while the GMAW and SAW plates have angular and bowing distortions.

Introduction

A classification of welding distortion into in-plane distortion (rotational, transverse, and longitudinal shrinkage) and out-of-plane distortion (buckling, angular, and longitudinal bending) is presented by Masubuchi (Ref. 1) — Fig. 1. The out-of-plane distortion significantly influences the required dimensional precision in structural components. In thin-section structures, buckling distortion is very common and the magnitude of distortion tends to be very large. Buckling causes loss

in structural integrity, dimension control, and increased fabrication costs due to poor fit-up between panels. This has a high impact on the shipbuilding, railroad, and aerospace industries where large thin panels are welded.

Buckling distortion due to welding occurs when the residual stress exceeds the critical buckling strength of the structure (Refs. 2–6). Typically, the longitudinal component of residual stress causes buckling. Longitudinal residual stresses are tensile at the weld region and change to compressive away from the welds.

Over the last 15 years, the finite element analysis method has been used to predict distortion and residual stress in fusion welding (Refs. 7–10). Welding-induced buckling of thin-walled structures has been investigated in Refs. 3, 11, 12. Friction stir welding has been modeled using three-dimensional visco-plastic modeling (Ref. 13) and fully coupled thermomechanical analyses (Ref. 14). However, these approaches do not account for the elastic component of stress and, therefore, cannot compute residual stress. Elasto-plastic models of FSW have been presented in Refs. 15–18, using a heat input model accounting for the thermal expansion caused by the heat generated from the friction at the contact surface between the tool and the material. Although

such models compute residual stress, they do not account for the effects of material movement caused by the spinning tool. Experimental techniques have been used to measure residual stress in butt joints in FSW specimens (Refs. 15–20).

This paper evaluates the propensity to buckling distortion of submerged arc welding (SAW), gas metal arc welding (GMAW), and friction stir welding (FSW) by comparing longitudinal residual stress measurements on HSLA65 plates welded by the three welding processes. The blind hole drilling method was used to measure residual stress and digital gauges were used to measure out-of-plane distortion at specific grid points. Graphs of the out-of-plane distortion measurements were generated to determine the type of welding distortion (angular, bowing, and buckling) for each plate. Analysis of the longitudinal residual stress distributions reveals a correlation of the residual stress distribution and welding distortion type.

Plate Dimensions and Welding Conditions

The specimens consist of two plates 28 × 9 in. (711.2 × 228.6 mm) butt joints welded together to form an 18-in.- (457.2-mm-) wide plate. All plates are ¼-in.- (6.35-mm-) thick HSLA-65 steel — Fig. 2. Two conventional arc and one friction stir welded plates were fabricated at Bath Iron Works and University of South Carolina, respectively. Table 1 lists the welding conditions for each type of weld. Case 1 is a double-pass, two-sided (bottom side first) submerged arc weld (SAW), and Case 2 is a single-pass, single-sided gas metal arc weld (GMAW) with a copper backing bar. Case 3 is a single-pass, single-sided friction stir weld. The edges of the plate were free during welding for the SAW and GMAW and restrained for the

KEYWORDS

Residual Stress
 Welding Distortion
 Buckling Distortion
 Bowing Distortion
 Angular Distortion
 Gas Metal Arc Welding
 Submerged Arc Welding
 Friction Stir Welding

S. R. BHIDE (srb252@psu.edu) is a graduate student, and P. MICHALERIS (pxm32@psu.edu) is an associate professor, Department of Mechanical and Nuclear Engineering, Pennsylvania State University, University Park, Pa. M. POSADA and J. DELOACH are with the Naval Surface Warfare Center, Carderock Division, Annapolis, Md.

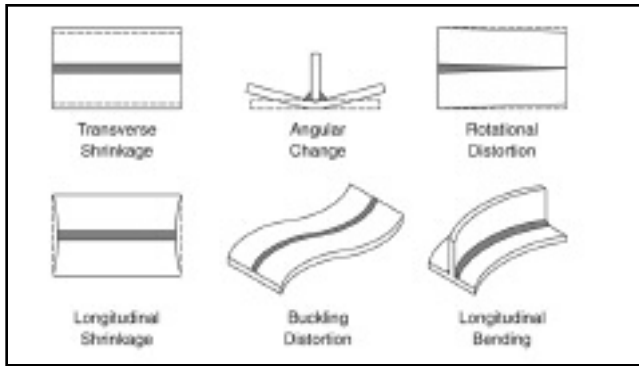


Fig. 1 — Types of welding distortion (Ref. 1).

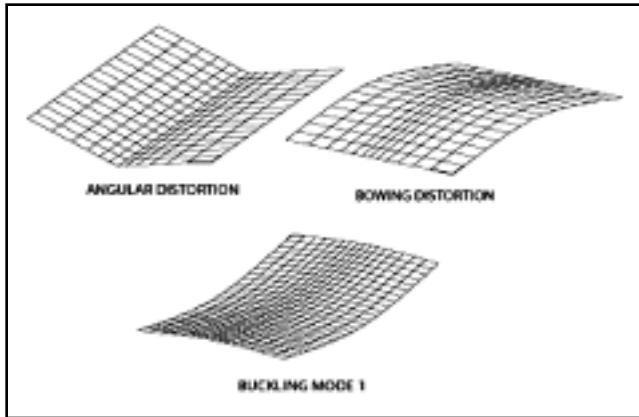


Fig. 3 — Types of out-of-plane distortion in butt-joint welded plates.

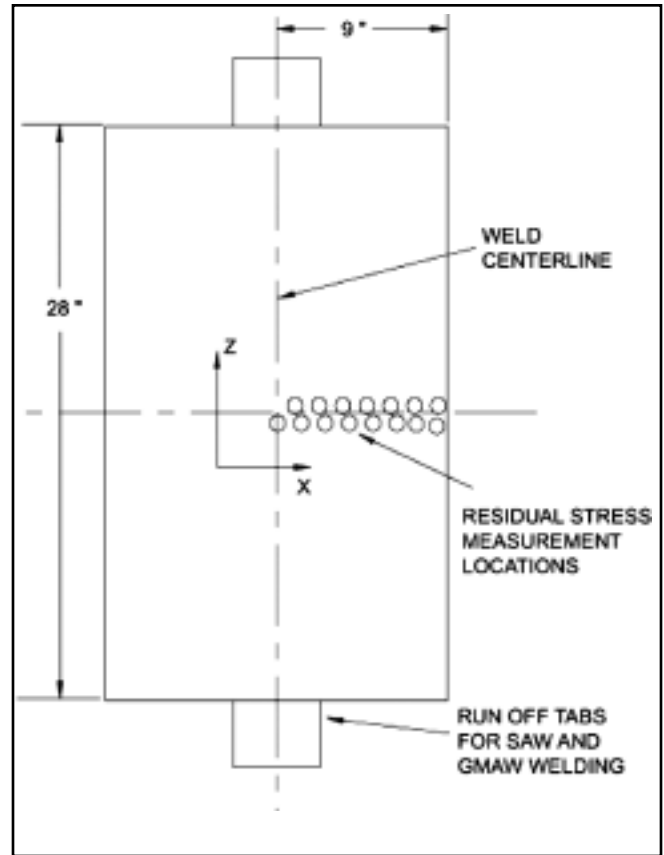


Fig. 2 — Geometry of plate.

FSW plate. Table 1 lists the total gross heat input of all processes. The heat input for the FSW was calculated based on the parameters of 6 in./min (2.54 mm/s), 3500 lb (15568.8 N) Z axis load and at 750 rpm that were used. All welds used a square butt-joint configuration and were fabricated in the flat position.

Distortion Types for Butt-Joint Welded Plates

Figure 3 illustrates the types of out-of-plane welding distortion in butt-joint welded plates. A plate with pure angular distortion is composed of two planes forming an angle at the weld centerline. A plate with pure bowing distortion has uniform longitudinal bowing. A plate with pure buckling distortion may deform into any of its buckling modes. The first mode is illustrated in Fig. 3, while higher modes are illustrated in Fig. 4. The buckling modes in Fig. 4 are generated by performing an eigenvalue buckling analysis using the commercial software *Abaqus* Version 6.3 for a plate with tensile longitudinal stress at the weld centerline and compressive elsewhere.

Minimization of potential energy results into a plate buckling into its lowest kinematically allowable mode. For exam-

ple, a free plate will buckle into the first mode. If the weld centerline is not allowed to bend (i.e., by welding a stiffener), it will buckle into the second mode.

Distortion Measurements

Figures 5–7 show the specimens for the three welding cases. In the SAW plate (Fig. 5), the edges of the plate move up, which is an indication of angular distortion. Also, the plate has a convex longitudinal bowing shape when viewed from the top. The distortion in the GMAW plate (Fig. 6) is of a similar nature as the SAW plate. The FSW plate (Fig. 7) viewed from the top has concave longitudinal and convex transverse bowing. The start and end of the plate move up while the edges of the plate move down. The combination of longitudinal and transverse bowing results into forming a saddle shape, which is indicative of buckling distortion — Fig. 3.

Out-of-plane distortion measurements were obtained at 40 points for each plate (Ref. 21). All measurements are in mm. Figure 8 illustrates plots of the out-of-plane, pre- and postweld distortion measurements. The relative distortion values were obtained by subtracting the preweld measurements from the postweld measurements and plotted in Fig. 9.

Evaluation of Buckling Distortion

To determine if a plate has buckling distortion, a correlation between the measured distortion and the first buckling mode is performed. However, eigenmodes are normalized displacement results, therefore the eigenmode results are scaled by a factor α . The correlation error E is computed as follows:

$$E = \left(\frac{\sqrt{\sum (\alpha\chi_1 - \chi_2)^2}}{n} \right) \quad (1)$$

where n is the number of measurement points.

Figure 10 depicts the error E for the three plates as a function of the scaling factor α . Low error E implies a good correlation between the measured distortion and the buckling mode indicating that buckling is present. The scaling factor α represents the magnitude of buckling distortion. The minimum error computed is 1.2653 ($\alpha = 4.5$), 1.4832 ($\alpha = 13$), and 0.2459 ($\alpha = 4.5$) for SAW, GMAW, and FSW, respectively. The error for the FSW plate is five times lower than the other cases. As the FSW plate shows very good correlation, it can be concluded that it has

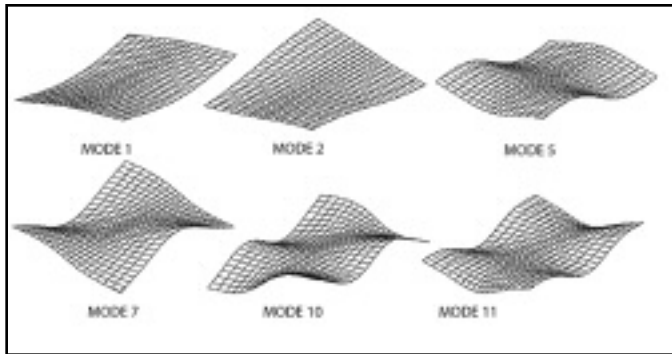


Fig. 4 — Modes of buckling distortion in butt-joint welded plates.



Fig. 5 — Submerged arc welded plate.



Fig. 6 — Gas metal arc welded plate.



Fig. 7 — Friction stir welded plate.

moderate buckling distortion (scaling factor of 4.5). The higher correlation error for GMAW and SAW plates indicates that the plates have primarily bowing and angular distortion. In summary, the distortion modes are as follows:

- SAW: angular and bowing distortion
- GMAW: angular and bowing distortion
- FSW: Buckling distortion of Mode 1.

Residual Stress Measurements

Residual Stress Measurement Methods

Several destructive and nondestructive methods are available to measure residual stress. The destructive method proposed by Norton and Rosenthal (Ref. 22) involves the removal of two thin slices of material from thick welds. Other destructive methods have been proposed by Gunnert (Ref. 23), which utilize pairs of measuring holes and incremental overcoring to release residual stress and by Ueda (Ref. 24), where an array of strain gauges is attached to one of the sample's longitudinal faces to measure residual stress. The non-destructive methods generally employed are X-ray diffraction and neutron diffraction. The common types of errors in X-ray diffraction are dependent on stress constant selection, microstructure, grain size, surface condition, etc. The applications,

Table 1 — Welding Conditions

Case	Process	Heat Input in kJ/in.	Consumables
Case 1	SAW	23.3 (S1) and 28.4 (S2)	EM-12K (Filler) and F7A2 (Flux)
Case 2	GMAW	28.6	MIL-70S-3 (Filler) 0.045 in. diameter
Case 3	FSW	35.9	None

Table 2 — Measured Longitudinal Residual Stress for Submerged Arc Welded Plate: Case 1

Top Side of the Plate		Bottom Side of the Plate	
X Coordinate from Center (mm)	Measured Longitudinal Residual Stress (MPa)	X Coordinate from Center (mm)	Measured Longitudinal Residual Stress (MPa)
12.5	520.81	12.7	534.88
25	204.48	22.2	51.3
45	39.71	38.1	-156.08
55	46.72	44.5	-176.39
97.5	62.4	60	-188.54
135	113.45	73	-192.29
185	147.51	89	-186.92
—	—	111	-155.13
—	—	127	-152.18
—	—	190	-113.76

limitations, and source of errors of the nondestructive methods for residual stress measurement are discussed in detail by Ruud (Ref. 25).

In this work, the blind hole drilling strain gauge method (Ref. 26) was se-

lected for measuring residual stress. It is one of the more successful and widely used semidestructive mechanical methods for experimental residual stress analysis (Refs. 27–29). This technique involves monitoring the change in strains produced

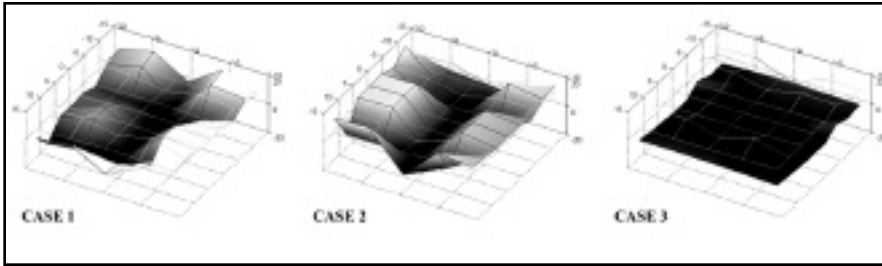


Fig. 8 — Preweld (grid) and postweld (solid) distortion measurements (Ref. 21).

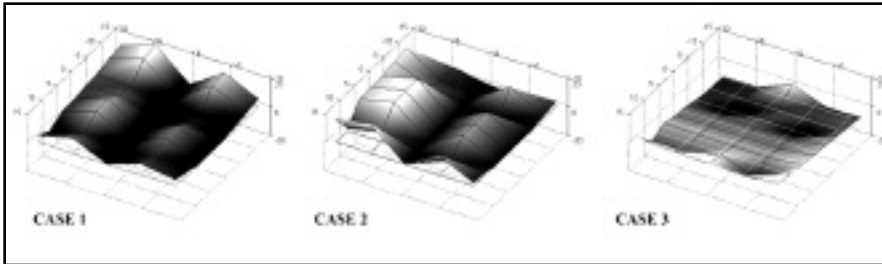


Fig. 9 — Relative distortion measurements (Ref. 21).

Table 3 — Measured Longitudinal Residual Stress for Gas Metal Arc Welded Plate: Case 2

Top Side of the Plate		Bottom Side of the Plate	
X Coordinate from Center (mm)	Measured Longitudinal Residual Stress (MPa)	X Coordinate from Center (mm)	Measured Longitudinal Residual Stress (MPa)
10	539.88	10	597.68
22	28.37	22.5	44.03
45	70.75	35	-84.08
65	-8.79	47.5	-79.73
95	-25.38	65	-77.73
135	-45.1	95	-102.417
165	0	135	-147.52
190	-37.02	180	-130

Table 4 — Measured Longitudinal Residual Stress for Friction Stir Welded Plate: Case 3

Top Side of the Plate		Bottom Side of the Plate	
X Coordinate from Center (mm)	Measured Longitudinal Residual Stress (MPa)	X Coordinate from Center (mm)	Measured Longitudinal Residual Stress (MPa)
-185	-88.03	-177	-3.3
-165	-51.08	-115	36.72
-140	-91.07	-95	85.1
-110	-73.76	-75	17.03
-85	-103.52	-44	41.9
-65	-34.52	-32	22.7
-35	5.244	-27.5	139.37
0	472.14	-10	566.41
22.5	170.54	10	478.04
50	-26.13	22.5	238
60	-52.66	32.5	59.41
80	-11.72	57.5	3.3
125	-117.14	78	6.36
140	-118.32	95	0.67
165	-142.1	115	19.38
190	-153.4	145	-3.3
—	—	198	3.94

when a small hole is drilled into a component containing residual stress. This change is measured using strain gauge rosettes and the residual stress is evaluated assuming elastic unloading.

The introduction of a hole (even of very small diameter) into a stressed body relaxes the stress at that location. This occurs because every normal to a free surface (the hole surface, in this case) is necessarily a principal axis on which the shear and normal stresses are zero. The elimination of these stresses on the hole surface changes the stress in the immediate surrounding region, causing local strains on the surface of the test object to change correspondingly. This principle is the foundation for the hole-drilling method of residual stress measurement, first proposed by Mathar (Ref. 30).

EA-06-062RE-120-SE rosette strain gauges manufactured by Vishay Micro-Measurements were used in this study. This is a general-purpose constantan grid open-faced strain gauge with 0.03-mm-thick flexible polyimide backing. The gauge length is 0.062 in. (1.6 mm), and the grid centerline diameter is 0.202 in. (51.3 mm). The gauge has a 0.08-in.- (2-mm-) diameter hole in the center for the drill to pass through. Calibration of the gauges is carried out using the procedure described in the manufacturer engineering data sheet U059-07 and technical note 503. This procedure follows the guidelines set by ASTM E837, *Determining Residual Stress by the Hole Drilling Strain Gauge Method* (Ref. 26). A pneumatically driven drill of 0.06 in. (1.6 mm) diameter is used for producing 0.07-in.- (1.778-mm-) deep blind holes. The principal residual stresses are calculated using the measured strain readings ϵ_1 , ϵ_2 , and ϵ_3 .

$$\sigma_{\max} = \frac{\epsilon_1 + \epsilon_2}{4A} - \frac{1}{4B} \sqrt{(\epsilon_3 - \epsilon_1)^2 + (\epsilon_3 + \epsilon_1 - 2\epsilon_2)^2} \quad (2)$$

$$\sigma_{\min} = \frac{\epsilon_1 + \epsilon_2}{4A} + \frac{1}{4B} \sqrt{(\epsilon_3 - \epsilon_1)^2 + (\epsilon_3 + \epsilon_1 - 2\epsilon_2)^2} \quad (3)$$

A and B are coefficients calculated on the basis of the strain gauge used and are dependent on the radius of the drill and the radius of the strain gauge used. The values of A and B used here are $-3.6857E-13$ and $-7.1428E-13$ (1/MPa), respectively. Longitudinal residual stress measurements are obtained on both the top and bottom surfaces of the plate along the central axis, transverse to the welding direc-

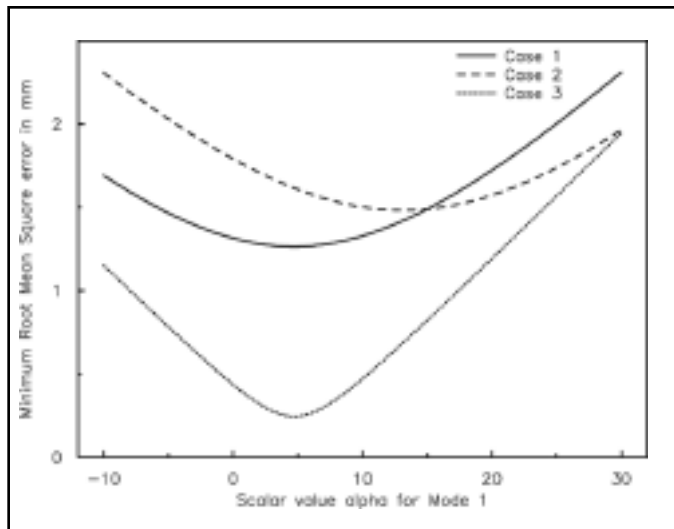


Fig. 10 — Comparison of RMS error for all plates for Mode 1.

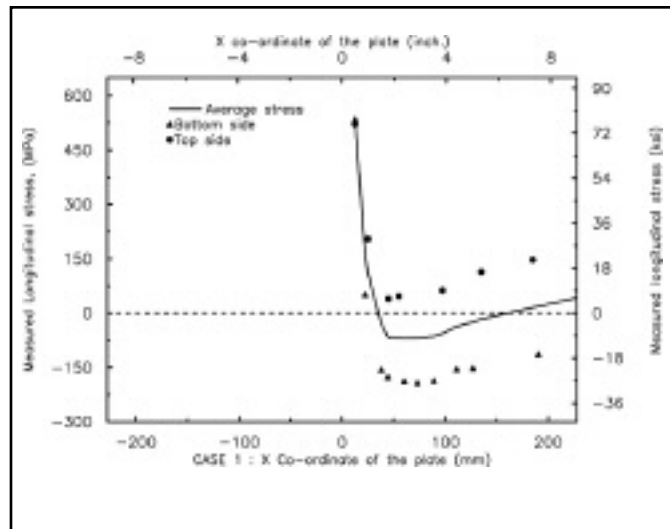


Fig. 11 — Measured longitudinal residual stresses for SAW plate.

tion. The small circles in Fig. 2 illustrate the locations of the measurements. The measurements were carried out only on one side of the weld centerline for the GMAW and SAW plates and both sides for the FSW plate.

Case 1: Submerged Arc Welded Plate

The residual stress measurements of the SAW plate (Fig. 5) are tabulated in Table 2 and plotted in Fig. 11. The plot shows that both the top and bottom surfaces have high tensile stresses near the weld that decrease sharply to an approximate distance of 25 mm from the weld centerline.

At 25 mm away from the weld centerline, the stress changes from tensile to compressive on the bottom surface. The magnitude of the compressive stress on the bottom side ranges from 192 MPa at 73 mm from the weld centerline to 114 MPa at 190 mm from the weld centerline. The stress at the top surface remains tensile throughout the entire length of one side of the weld. The measurements range from 40 to 150 MPa at distances of 45 to 185 mm from the weld centerline, respectively.

The large through-thickness stress variation suggests longitudinal bowing distortion, while the nearly linear shift from compressive stress adjacent to the weld to tensile at the edge suggests angular distortion. The through-thickness longitudinal stress variation is uniform from the center to the ends of the plate, indicating uniform longitudinal bowing curvature in the plate.

Case 2: Gas Metal Arc-Welded Plate

The residual stress measurements of the GMAW plate (Fig. 6) are tabulated in Table 3 and plotted in Fig. 12. This plate

has the highest tensile stress present at the weld region. The tensile stress decreases sharply from the weld centerline to approximately 25 mm away from the weld centerline. Beyond 25 mm from the weld centerline, the stress changes from tensile to compressive.

The deviation between the top and bottom surface measurements is less compared to that of SAW. The deviation is also uniform suggesting longitudinal bowing curvature for the plate. Since the plate has less angular distortion, the stresses at the ends of the plate remain compressive.

Case 3: Friction Stir Welded Plate

The residual stress measurements of the FSW plate (Fig. 7) are tabulated in Table 4 and plotted in Fig. 13. The plot shows that high tensile stress is present and decreases as the distance increases from the weld centerline. The longitudinal stress distribution is asymmetric.

At an approximate distance of 50 mm from the weld centerline, the stress becomes compressive for measurements taken at the top surface. The stress at the bottom surface is negligible. The top sur-

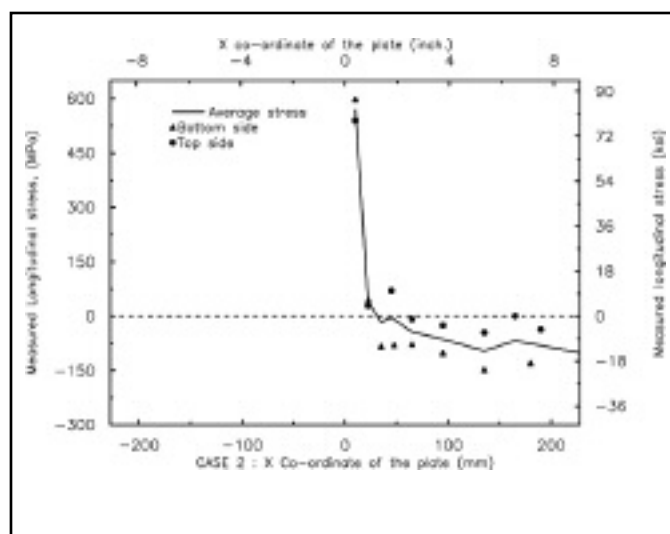


Fig. 12 — Measured longitudinal residual stresses for GMAW plate.

face has constant compressive residual stress. The average stress values of the top and bottom surfaces, shown by the solid line, are compressive for measurements beyond 50 mm from the weld centerline. It can be seen that the through-thickness stress variation in this case is not uniform but increases at the ends of the plate. This variation is attributed to the fact that the edges of the plate have different longitudinal curvature compared to the relatively straight centerline. This is a result of mode 1 buckling — Fig. 3.

The friction stir-welded plate has the highest heat input as compared to the other two welding types (Table 1). However, in FSW, the heat is distributed in a wider area over the weld resulting in no

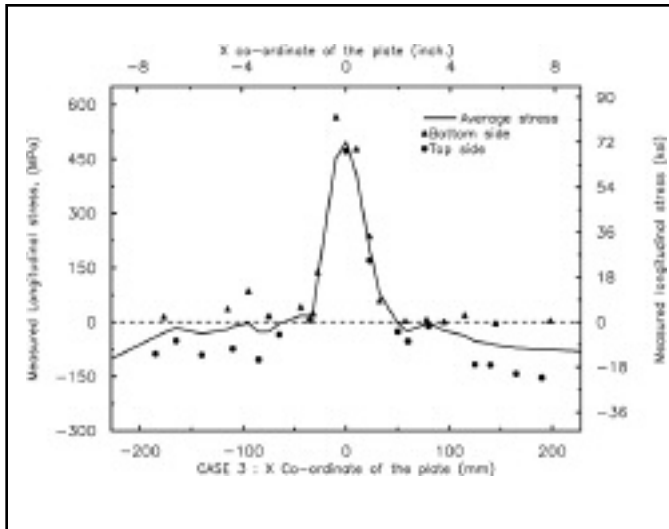


Fig. 13 — Measured longitudinal residual stresses on FSW plate.

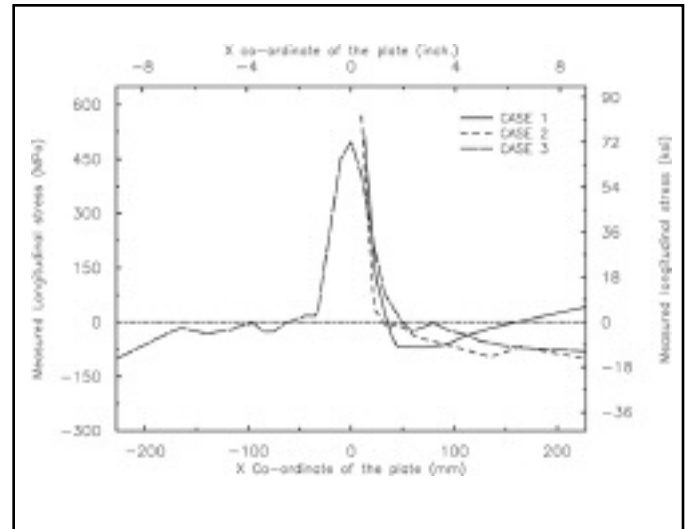


Fig. 14 — Average measured longitudinal residual stress.

melting. Therefore, the temperature spatial gradient and cooling rates are different in FSW than GMAW and SAW.

Comparison of the Types of Welding

- The GMAW and SAW plates have higher tensile stresses near the center of the weld (513 and 568 MPa) as compared to FSW plate (480 MPa). However, the FSW plate has a wider tensile zone (100 mm) at the weld centerline as compared to that generated by the arc processes (50 mm).

- The FSW plate has the highest longitudinal compressive stress at the plate's free edges (-153.4 MPa, Table 4) making it most susceptible to buckling distortion.

- Comparison of the welding heat input in Table 1 and peak compressive residual stress in Fig. 14 indicates that there may be a correlation between compressive residual stress and welding heat input. Such a correlation has been observed in arc welding processes (Ref. 12). However, more data are needed for FSW to confirm this correlation.

- Since the arc processes were performed without any edge restraints, the GMAW and SAW plates show considerable angular distortion (6 and 12 mm, respectively) as compared to the FSW plate (3 mm), where the edge restraints limit angular distortion (Refs. 31, 32).

- The through the thickness stress variations for GMAW and SAW processes were uniform, suggesting uniform longitudinal bowing. In the FSW case, however, the through the thickness variation is less at the weld centerline and gradually increases toward the edges, suggesting non-uniform bending, which is indicative of buckling.

Conclusions

Experimental comparison of the SAW, GMAW, and FSW processes was performed in terms of the longitudinal residual stress and out-of-plane distortion. Different fixturing conditions resulted in significant magnitude of angular distortion in SAW and GMAW plates than the FSW plate.

However, the FSW plate results show high compressive stress at the edges indicating the process being more prone to buckling. In fact, the test plate did buckle.

Larger plates under the same welding conditions are expected to result in significantly higher buckling distortion if FSW is used instead of SAW or GMAW. The longitudinal residual stress measurements indicate that there is a correlation between the welding heat input and the longitudinal residual stress.

Further work is needed using FSW plates of different heat inputs to explore this correlation and to develop methodologies for minimizing residual stress.

Acknowledgments

The authors would like to acknowledge funding for this work from ONR, award number N000140010645 and program manager Julie Christodoulou, and from the DUS&T program funded by ONR by George Yoder and Julie Christodoulou.

References

1. Masubuchi, K. 1980. *Analysis of Welded Structures*. Pergamon Press, Oxford.
2. Ueda, Y., Kim, Y. C., and Yuan, M. G. 1989. A predictive method of welding residual stress using source of residual stress (report I) characteristics of inherent strain (source of

residual stress). *Transactions of JWRI* 18(1): 135-141.

3. Tsai, C. L., Park, S. C., and Cheng, W. T. 1999. Welding distortion of a thin-plate panel structure. *Welding Journal* 78: 156-s to 165-s.

4. Michaleris, P., and DeBicari, A. 1996. Prediction of welding distortion. Presented at 77th Annual AWS Convention.

5. Vanli, O. A., and Michaleris, P. 2001. Distortion analysis of welded stiffeners. *Journal of Ship Production* 17(4): 226-240.

6. Deo, M. V., Michaleris, P., and Sun, J. 2003. Prediction of buckling distortion of welded structures. *Science and Technology in Welding* 8(1): 55-61.

7. Goldak, J., Chakravarti, A., and Bibby, M. 1984. A new finite element model for welding heat sources. *Metallurgical Transactions B*, 15B: 299-305.

8. Leblond, J. B., and Devaux, J. 1984. A new kinetic model for anisothermal metallurgical transformations in steels including effect of austenite grain size. *Acta Metall* 32(1): 137-146.

9. Watt, D. F., Coon, L., Bibby, M. J., Goldak, J., and Henwood, C. 1988. An algorithm for modeling microstructural development in weld heat-affected zones. *Acta Metall* 36(11): 3029-3035.

10. Henwood, C., Bibby, M., Goldak, J., and Watt, D. 1988. Coupled transient heat transfer — microstructure weld computations, part B. *Acta Metall* 36(11): 3037-3046.

11. Murakawa, H., Ueda, Y., and Zhong, X. M. 1995. Buckling behavior of plates under idealized inherent strain. *Transactions of JWRI* 24(2): 87-91.

12. Michaleris P., and DeBiccar, A. 1997. Prediction of welding distortion. *Welding Journal* 76(4): 172-180.

13. Ulysse, P. 2002. Three-dimensional modeling of the friction stir-welding process. *International Journal of Machine Tools and Manufacture* 42: 1549-1557.

14. Ulysse, P. 2002. Three-dimensional

modeling of the friction stir welding process. *International Journal of Machine Tools and Manufacture* 48: 1549–1557.

15. McClure, J. C., Tang, W., Murr, L. E., Guo, X., Fang, Z., and Gould, J. E. 1998. A thermal model of friction stir welding. *Proceedings of the 5th International Conference: Trends in Welding Research*, pp. 590–595, Pine Mountain, Ga.

16. Gould, J., and Feng, Z. 1998. Heat flow model for friction stir welding of aluminum alloys. *Journal of Materials Processing & Manufacturing Science* 7: 185–194.

17. Chao, Y. J., Qi, X., and Tang, W. 2003. Heat transfer in friction stir welding — experimental and numerical studies. *Journal of Manufacturing Science and Engineering* 125: 138–145.

18. Frigaard, O., Grong, O., and Milding, O. T. 2001. A process model for friction stir welding of age hardening aluminum alloys. *Metallurgical and Materials Transactions A: Physical Metallurgy and Materials Science* 32: 1189–1200.

19. Sutton, M. A., Reynolds, A. P., Wang, D.-Q., and Hubbard, C. R. 2002. A study of residual stresses and microstructure in 2024-t3 aluminum friction stir butt welds. *Journal of*

Engineering Materials and Technology 124: 215–221.

20. Sutton, M. A., Reynolds, A. P., Wang, D.-Q., and Hubbard, C. R. 2002. A study of residual stresses and microstructure in 2024-t3 aluminum friction stir butt welds. *Journal of Engineering Materials and Technology* 124: 215–221.

21. Posada, M., DeLoach, J., Reynolds, A. P., Bhide, S. R., and Michaleris, P. 2003. Evaluation of friction stir welded HSLA-65. In *Advanced Marine Materials: Technology and Applications*, London, UK, Royal Institution of Naval Architects.

22. Rosenthal, D., and Norton, J. T. 1945. A method for measuring triaxial residual stresses in plates. *Welding Journal* 24: 295–307.

23. Gunnert, R. 1961. Residual stresses. Special symposium on the behavior of welded structures, University of Illinois Engineering Experiment Station, Urbana, Ill., pp. 167–201.

24. Ueda, Y., Fukuda, K., Nakacho, K., and Endo, S. 1975. A new measuring method of residual stresses with the aid of finite element method and reliability of estimated values. *Trans. Japan Welding research Institute* 4(2): 122–131.

25. Ruud, C. O. 1982. A review of selected

nondestructive methods for residual stress measurement. *NDT International* 15: 15–23.

26. *Determining residual stresses by the hole drilling strain gauge method*. ASTM Standard E837.

27. Rendler, N. J., and Vigness, I. 1966. Hole-drilling strain-gauge method of measuring residual stresses. *Exp Mech* 6: 577–586.

28. Gupta, B. 1973. Hole-drilling technique: modifications in the analysis of residual stresses. *Exp Mech* 13: 45–48.

29. Zuccarello, B. 1999. Optimal calculation steps for the evaluation of residual stress by the incremental hole-drilling method. *Exp Mech* 39: 117–124.

30. Mathar, J. 1934. Determination of initial stresses by measuring the deformation around drilled holes. *Trans. ASME* 56: 249–254.

31. Michaleris, P., and Sun, X. 1997. Finite element analysis of thermal tensioning techniques mitigating weld buckling distortion. *Welding Journal* 76(11): 451–457.

32. Deo, M. V., and Michaleris, P. 2003. Mitigation of welding induced buckling distortion using transient thermal tensioning. *Science and Technology in Welding* 8(1): 49–53.